Electron g - 2, Entanglement, and Trapped-Ion Quantum Information Processing

D. J. Wineland

Time and Frequency Division, NIST, Boulder, CO 80305-3328

Abstract. Experiments on quantum-state synthesis of trapped ions and their connection to trapped-electron $g - 2$ experiments are discussed briefly. The trapped-ion work has the overall goal of performing large-scale quantum information processing; however, the techniques employed can also be applied to fundamental tests and demonstrations of quantum mechanical principles, as well as to the improvement of quantum-limited measurements.

INTRODUCTION

On this occasion where we honor Prof. Hans Dehmelt upon his retirement we can see, in many ways, his influence upon the work that we currently pursue. In research devoted to the possibility of processing quantum information using trapped ions, this influence is rather direct. For example, the trapped-ion method follows his pioneering work on its applications in atomic physics. In addition, the key entangling operation needed for quantum information processing is a close analog to the "$g - 2$" measurement technique that was used for the high-precision measurements of the electron and positron g-factors in Prof. Dehmelt's group at the University of Washington. Before discussing this connection, we first recall some of the basic ideas involved in the electron $g - 2$ measurement.

G - 2 AND SPIN/MOTION ENTANGLEMENT

Consider an electron in a magnetic field $\vec{B}_0$ as shown schematically in Fig. 1. The energy of the electron's spin magnetic moment in this field is given by $H_S = -\vec{\mu} \cdot \vec{B}_0 = -g\mu_B B_0 m_S$ where $g \simeq -2.002$ is the electron g-factor, μ_B is the Bohr magneton, and $m_S \in \{-1/2, +1/2\} \equiv \{\downarrow, \uparrow\}$ is the electron's spin eigenvalue with respect to a quantization axis determined by $\vec{B}_0$. The electron's motion in a direction perpendicular to $\vec{B}_0$ is described by its cyclotron orbit (in the x-y plane of Fig. 1) at frequency

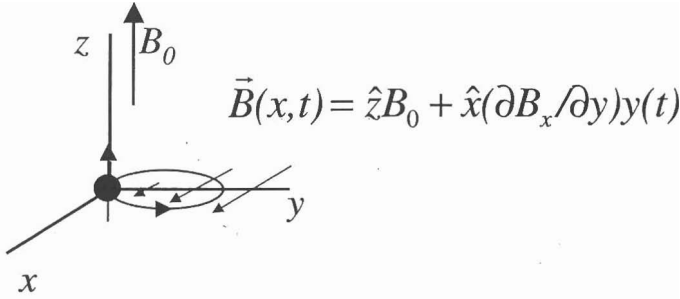$$\vec{B}(x,t) = \hat{z}B_0 + \hat{x}(\partial B_x/\partial y)y(t)$$

FIGURE 1. Schematic representation of the motion of an electron in a strong uniform magnetic field plus a gradient field acting as a perturbation. When the electron traverses its cyclotron orbit, it sees an oscillating magnetic field parallel to $\hat{x}$ as it moves through the field gradient. If this field is modulated at $|g| - 2$ times the cyclotron frequency ω_C, where g is the electron g-factor, the electron experiences an oscillating magnetic field that flips its spin.

$\omega_C = eB_0/m_e$ where e and m_e are the electron's charge and mass. Assume that a weaker magnetic field gradient is also applied to the electron, where this additional field is perpendicular to $\vec{B}_0$ as indicated in the figure. As the electron traverses its cyclotron orbit, it sees an oscillating component of the magnetic field in the $\hat{x}$ direction due to its motion in the field gradient. Now assume that this field gradient oscillates sinusoidally at the frequency $\omega_S - \omega_C$, where ω_S is the electron's spin-flip frequency. We represent the y-component of the electron's motion and the field gradient as

$$y(t) = Y_0 \cos(\omega_C t), \quad \partial B_x/\partial y = B' \cos((\omega_S - \omega_C)t). \tag{1}$$

If we substitute these expressions into the expression for the total field (indicated in the figure), we find that the electron sees the field

$$\vec{B}(t) = \hat{z}B_0 + \hat{x}(B'Y_0/2)\left[\cos(\omega_S t) + \cos((\omega_S - 2\omega_C)t)\right]. \tag{2}$$

The last term in this equation is non-resonant and may be neglected. However, the term that oscillates as $\cos(\omega_S t)$ causes the spin to flip. Hence, by modulating the gradient field at a frequency equal to the "$g - 2$ frequency" $\omega_S - \omega_C = (|g| - 2) \times \omega_C$, we cause the spin and cyclotron motion to exchange energy. After the cyclotron motion has radiatively re-thermalized with the environment, the change in averaged magnetic moment energy (spin plus cyclotron magnetic moment energy) is detected through a shift in the electron's axial frequency [1], thereby signaling the $g - 2$ resonance condition.

If we describe this situation treating both the spin and motion quantum mechanically, we write the system Hamiltonian as

$$H = -\vec{\mu} \cdot \vec{B} = H_0 + H_I, \qquad H_0 = -\frac{1}{2}g\mu_B B_0 \sigma_z + \hbar\omega_C a_C^\dagger a_C,$$

$$H_I = -\frac{1}{2}g\mu_B(\partial B_x/\partial y)y_0(a_C + a_C^\dagger)(\sigma^+ + \sigma^-), \qquad (3)$$

where $\sigma^+ = (\sigma_x + i\sigma_y)/2$ and $\sigma^- = (\sigma_x - i\sigma_y)/2$ are the raising and lowering operators for the spin, and σ_x, σ_y, and σ_z are the usual Pauli matrices. Y_0 has been replaced by the position operator $y_0(a_C + a_C^\dagger)$, where a_C and $a_C^\dagger$ are the lowering and raising operators for the cyclotron motion and y_0 represents the zero-point amplitude of the motion. When $\partial B_x/\partial y$ is modulated at the $g-2$ frequency, the resonant (and dominant) part of H_I is proportional to $a_C\sigma^+ + a_C^\dagger\sigma^-$, an interaction that entangles the spin and cyclotron motion. For pure states of two quantum systems, such as the spin and cyclotron motion in the present context, entanglement means that the wavefunction describing the overall system cannot be written as a direct product of wave functions of the separate systems. One consequence of entanglement is that measurements on one system are correlated with those on the other system. Logic gates used in quantum computers generate entanglement between quantum bits or "qubits" and, as we will see below, an interaction entirely analogous to that in Eq.(3) is the basis for entanglement and quantum logic gates between atomic ion qubits.

BASIC IDEAS OF TRAPPED-ION QUANTUM COMPUTATION

Efforts to realize the elements of quantum computation (QC) experimentally with trapped atomic ions have been stimulated in large part by a 1995 proposal by Cirac and Zoller [2]. In this scheme, ions confined in a linear RF (Paul) trap are cooled and form a stable spatial array whose motion is described by collective normal modes. Two internal levels in each ion form a qubit (referred to as a spin qubit below). The spacing ($> 1\ \mu m$) between ions is typically large enough that the direct coupling of internal states of ions is negligible, thereby precluding logic gates based on internal-state interactions. To overcome this limitation, Cirac and Zoller suggested cooling the ions to their motional ground state and using the ground and first excited state of a particular motional mode as a qubit (motion qubit). The motional mode can act as a data bus to transfer information between ions by first mapping the spin qubit state of a particular ion onto the selected motion qubit with a laser beam focused onto that ion. The ability to construct a logic gate between the motion qubit and another selected spin qubit, coupled with the

ability to perform single-spin qubit rotations provides the necessary requirements for universal quantum computation [3, 4].

The ion-trap scheme satisfies the main requirements for a quantum computer as outlined by DiVincenzo [5]: (1) a scalable system of well-defined qubits, (2) a method to reliably initialize the quantum system, (3) long coherence times, (4) existence of universal gates, and (5) an efficient measurement scheme. Most of these requirements have been demonstrated experimentally; consequently, ion-trap quantum information processors are studied in several laboratories. Here, we focus on experiments carried out at NIST but note that similar work is being pursued at Aarhus, Almaden (IBM), Hamburg, Hamilton (Ontario, McMaster Univ.), Innsbruck, Los Alamos (LANL), University of Michigan, Garching (MPI), Oxford, and Teddington (NPL, U.K.). For brevity, we discuss only one example of a trapped-ion logic gate and indicate steps being taken towards scaling to a large system.

COHERENT QUANTUM CONTROL

The key entangling operation in the 1995 Cirac/Zoller scheme for QC, and other schemes that rely on the ions' motion, is an operation that coherently couples a spin qubit with the motion in a spin-state-dependent way. Assume that the spin qubit has a ground state labeled $|\downarrow\rangle$ and a higher metastable state labeled $|\uparrow\rangle$ that are separated in energy by $\hbar\omega_0$. First assume that single-photon transitions between these levels can be excited with a focused laser beam. For simplicity, we will assume electric dipole transitions, but this is easily adapted to other cases such as electric quadrupole transitions as in the experiments at Innsbruck [6]. The interaction between an ion and the electric field of the laser beam can be written as

$$H_I(t) = -\vec{d} \cdot \vec{E} = -\vec{d} \cdot E_0 \hat{\varepsilon}_L \cos(k\tilde{z} - \omega_L t + \phi), \qquad (4)$$

where $\vec{d}$ is the electric dipole operator, $\tilde{z}$ is the ion position operator for displacements from the ion's equilibrium position (expanded in terms of normal mode operators), $\hat{\varepsilon}_L$ is the laser beam polarization, k is the laser beam's k-vector (taken to be parallel to $\hat{z}$, the axis of the trap), ω_L is the laser frequency, and ϕ is the phase of the laser field at the mean position of the ion. E_0 is the laser beam electric field amplitude at the ion, which is assumed to be classical. We characterize the laser field's polarization with respect to a magnetic field $\vec{B}_0$ that sets the quantization axis for the ions. The polarization is expressed in terms of left circular ($\hat{\sigma}_-$), linear ($\hat{\pi}$), and right circular ($\hat{\sigma}_+$) polarizations, so that $\hat{\varepsilon}_L = e_- \hat{\sigma}_- + e_0 \hat{\pi} + e_+ \hat{\sigma}_+$ with $|e_-|^2 + |e_0|^2 + |e_+|^2 = 1$. The dipole operator $\vec{d}$ is proportional to $\sigma^+ + \sigma^-$, where $\sigma^+ \equiv |\uparrow\rangle\langle\downarrow|, \sigma^- \equiv |\downarrow\rangle\langle\uparrow|$. We take $\tilde{z} = z_0(a + a^\dagger)$, where a and $a^\dagger$ are the lowering and raising operators for the

harmonic oscillator associated with the selected motional mode (frequency ω_z) and z_0 is the extension of the ground-state wavefunction for the particular ion (and mode) being addressed. We assume all other z modes are cooled to and remain in their ground states and for simplicity have neglected them in $\tilde{z}$. In the Lamb-Dicke limit, where the extent of the ion's motion is much less than $\lambda/2\pi = 1/k$, we can write Eq. (4) (in the interaction frame, and making the rotating wave approximation (see for example, ref. [10])) as

$$H_I \simeq \hbar(\Omega e^{i\phi})\sigma^+ e^{-i(\omega_L-\omega_0)t}[1+i\eta(ae^{-i\omega_z t}+a^\dagger e^{i\omega_z t})]+h.c. \tag{5}$$

Here, $\Omega \equiv -E_0\langle\uparrow|\vec{d}\cdot\hat{\varepsilon}_L|\downarrow\rangle/(2\hbar)$ and $\eta = kz_0$ is the Lamb-Dicke parameter ($\ll 1$ in the Lamb-Dicke limit).

For certain choices of ω_L, H_I is resonant and the spin and motion can be coupled efficiently. For example, when $\omega_L = \omega_0 - \omega_z$, $H_I \simeq i\eta\hbar(\Omega e^{i\phi})\sigma^+ a + h.c.$ This is usually called the "red-sideband" coupling and is formally equivalent to the Jaynes-Cummings Hamiltonian from quantum optics (see, for example, Ref. [7]). As noted above, it is essentially the same interaction used in the $g-2$ experiments. Here, $|\downarrow\rangle \to |\uparrow\rangle$ transitions are accompanied by $|n\rangle \to |n-1\rangle$ motional mode transitions. When $\omega_L = \omega_0 + \omega_z$ (the "blue sideband" frequency), $H_I \simeq i\eta\hbar(\Omega e^{i\phi})\sigma^+ a^\dagger + h.c.$, and $|\downarrow\rangle \to |\uparrow\rangle$ transitions are accompanied by $|n\rangle \to |n+1\rangle$ transitions. When $\omega_L = \omega_0$, $H_I \simeq \hbar(\Omega e^{i\phi})\sigma^+ + h.c.$ and $|\downarrow\rangle \to |\uparrow\rangle$ transitions do not change n. These "carrier" transitions are used to perform the single spin-qubit rotations.

Raman transitions

Some experiments use two ground-state hyperfine levels as qubits. Coherent transitions between these levels can be implemented with two laser beams that drive coherent two-photon stimulated-Raman transitions. For this case, in Eq. (5), k must be replaced by the difference $\Delta k = |\vec{k}_1 - \vec{k}_2|$ between k-vectors for the two Raman beams (again assumed to be parallel to $\hat{z}$), ω_L and ϕ are replaced by $\omega_1 - \omega_2$ and $\phi_1 - \phi_2$, the frequency difference and phase difference between the laser beams at the mean position of the ion, and $\Omega e^{i\phi}$ is replaced by the resonant two-photon Raman Rabi rate

$$\Omega e^{i\phi} \leftrightarrow \frac{e^{i(\phi_1-\phi_2)}}{4\hbar^2}\sum_i \langle\uparrow|\vec{d}\cdot E_2\hat{\varepsilon}_2|i\rangle\langle i|\vec{d}\cdot E_1\hat{\varepsilon}_1|\downarrow\rangle/\Delta_i. \tag{6}$$

In this expression, the subscripts denote the two laser beams, $|i\rangle$ are the (virtual, electronically excited) intermediate states of the Raman process, and Δ_i are the detunings of the Raman beams as indicated in Fig. 2. We have assumed $\Delta_i \gg \gamma_i$, where γ_i are the decay rates from the intermediate states. With these substitutions, Eq. (5) applies in the
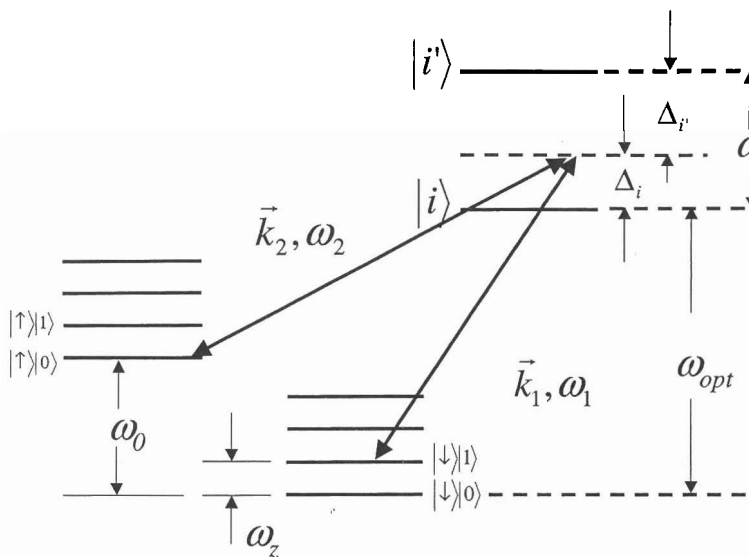
FIGURE 2. Schematic representation of relevant energy levels for stimulated-Raman transitions (not to scale). Shown are two ground-state hyperfine levels ($|\downarrow\rangle$ and $|\uparrow\rangle$) for one ion, two (of possibly many) excited levels ($|i\rangle$ and $|i'\rangle$), and the harmonic oscillator levels for one mode of motion. Typically, $\omega_z \ll \omega_0 \ll \Delta_i, \Delta_{i'}, \omega_F \ll \omega_{opt}$, where ω_{opt} is an optical frequency.

Lamb-Dicke limit, where the Lamb-Dicke parameter is now given by $\eta \equiv \Delta k z_0 \ll 1$. For brevity, we will specialize to the stimulated-Raman transition case in what follows.[1]

When the difference frequency of the Raman beams is tuned to resonance with the red or blue sidebands or carrier, the interaction leads to the coherent evolution

$$|\downarrow\rangle|n\rangle \rightarrow \cos(\Omega_{n,n'}t)|\downarrow\rangle|n\rangle - ie^{i\phi}\sin(\Omega_{n,n'}t)|\uparrow\rangle|n'\rangle \qquad (7)$$

and

$$|\uparrow\rangle|n\rangle \rightarrow -ie^{-i\phi}\sin(\Omega_{n,n'}t)|\downarrow\rangle|n\rangle + \cos(\Omega_{n,n'}t)|\uparrow\rangle|n'\rangle. \qquad (8)$$

When $n' = n \pm 1$ (blue or red sidebands), $\Omega_{n,n'} \equiv \eta\Omega(n_>)^{1/2}$, where $n_>$ is the greater of n or n'. In Fig. 2, we show a red sideband transition for $n = 1$. When the duration of this operation is adjusted to give a π pulse, the mapping from the spin qubit to motion qubit required in the Cirac/Zoller scheme $(\alpha|\downarrow\rangle + \beta|\uparrow\rangle)|0\rangle \rightarrow |\downarrow\rangle(\alpha|0\rangle + \beta|1\rangle)$ is executed.

---

[1] In principle, we could drive hyperfine carrier and sideband transitions with single photons at frequencies ω_0 and $\omega_0 \pm \omega_z$. However, in practice, attainable field gradients appear to be relatively small and the resulting small values of η would lead to slow sideband transition Rabi rates[8, 9].

From expressions (7) and (8) the entanglement between the spin and motion is evident since the final state cannot in general be factored into the product of spin and motional wavefunctions. Carrier transitions can also be described by these expressions, where $n = n'$ and $\Omega_{n,n'} = \Omega$.

In order to keep the duration of an entangling operation relatively short, $\Omega_{n,n'}$ for $n \neq n'$ cannot be too small relative to $\Omega_{n,n}$. Therefore η must be chosen large enough that our interaction does not rigorously satisfy the Lamb-Dicke criterion and correction factors must be added to the expressions for the Rabi frequencies $\Omega_{n,n'}$. These correction factors, which can be called Debye-Waller factors [10], have been observed by Meekhof et al. [11] and also form the basis for a controlled-not (CNOT) gate between motion and spin discussed below.

State initialization and detection

To initialize the qubits for each experiment, we use a combination of internal-state optical pumping (to pump to the $|\downarrow\rangle$ state) and sideband laser cooling to optically pump the motional modes to their ground states [6, 12, 13, 14]. As in many atomic physics experiments, the observable in the ion-trap experiments is the ion's spin qubit state. We can efficiently distinguish $|\downarrow\rangle$ from $|\uparrow\rangle$ using a cycling transition to implement "electron-shelving" [15, 16] detection.

GATES

Equations (7) and (8) illustrate a basic source of entanglement in ion experiments from which universal logic gates have been constructed. For example, a CNOT and π-phase gate between the motion and spin qubit for a single ion have been demonstrated [10, 17]. Also, using the scheme suggested by Sørensen and Mølmer [18, 19] and Solano et al. [20], a universal gate between two spin qubits has been realized [21, 22]. Here, another example of trapped-ion quantum gate is described.

Controlled-NOT "wave-packet" gate

Recently, a new kind of CNOT gate between the motion qubit (control bit) and spin qubit (target bit) that was proposed in Ref. [23] has been realized experimentally [24]. A CNOT gate toggles or leaves unaltered the state of the target bit depending on the state of the control bit. This gate described here uses carrier transitions and relies on

Debye-Waller correction factors [10] to provide the conditional dynamics for the gate. Including these correction factors, the carrier Rabi frequencies now depend on n:

$$\Omega_{n,n} = \Omega e^{-\eta^2/2} L_n(\eta^2), \tag{9}$$

where $L_n(X)$ is the Laguerre polynomial of order n. For the lowest three values of n, we have

$$L_0(\eta^2) = 1, \quad L_1(\eta^2) = 1 - \eta^2, \quad L_2 = 1 - 2\eta^2 + \eta^4/2. \tag{10}$$

The spin (target) qubit was formed from the $2s\,^2S_{1/2}, |F = 2, m_F = -2\rangle \equiv |\downarrow\rangle$ and $|F = 1, m_F = -1\rangle \equiv |\uparrow\rangle$ ground state hyperfine levels in $^9\text{Be}^+$. For the motional (control) qubit states we chose the $|n = 0\rangle$ and $|n = 2\rangle$ Fock states of the axial (z) motion of the ion in a linear Paul trap [25]. Therefore the four basis states for the spin and motion qubit were $|\downarrow\rangle|0\rangle, |\downarrow\rangle|2\rangle, |\uparrow\rangle|0\rangle$, and $|\uparrow\rangle|2\rangle$. To construct the CNOT gate we chose $\eta^2 = 0.129$, corresponding to $\omega_z/2\pi = 3.51$ MHz. This gave $\Omega_{0,0}/\Omega_{2,2} = 4/3$. By choosing the interaction time such that $\Omega_{0,0}t = 2\pi$, we realize the transformations $|\downarrow\rangle|0\rangle \rightarrow |\downarrow\rangle|0\rangle$, $|\uparrow\rangle|0\rangle \rightarrow |\uparrow\rangle|0\rangle$, $|\downarrow\rangle|2\rangle \rightarrow i|\uparrow\rangle|2\rangle$, and $|\uparrow\rangle|2\rangle \rightarrow i|\downarrow\rangle|2\rangle$. Up to phase factors that can be corrected by single-ion qubit rotations (or accounted for in software[2]), this gate is the CNOT gate. The gate operation is depicted schematically in Fig. 3.

This gate, when acting on eigenstates (as shown in the figure) acts like a classical gate. However it can also act on superposition states [24] (decidedly nonclassical), which leads to entanglement. Compared to the previously realized CNOT gate between motion and spin [17] this gate has the advantages that (1) it requires only one step instead of three, (2) it does not require an auxiliary internal state, and (3) it is immune to Stark shifts caused by coupling to "spectator" states [24] (here, two-photon Stark shifts from coupling to non-resonant sideband transitions). This gate is fundamentally different from previously demonstrated gates in that it relies on the wave-packet nature of the ions. To obtain the correct interaction with the laser, we must average the laser field over the extent of the ion's wave packet (giving the Debye-Waller factors) rather than assuming it is a point particle.

TOWARDS LARGE-SCALE QUANTUM COMPUTATION

Although simple logic operations among a few ion qubits have been demonstrated, a viable quantum computer must include a way to scale to very large numbers of qubits

---

[2] The transformation looks like the desired CNOT operation followed by a $\pi/2$ phase shift ($i = e^{i\pi/2}$) on the $|2\rangle$ state of the motion qubit. This phase shift can be removed by shifting the phase of the relevant laser oscillator for the next operation on the motion qubit.
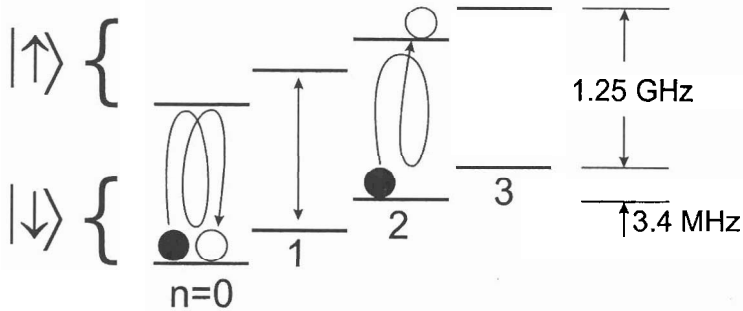
FIGURE 3. Schematic of the trapped ion levels and CNOT gate operation. Shown here are the trapped ion motional levels (separated in energy by $h \times 3.4$ MHz, where h is Planck's constant) and internal spin states $|\uparrow\rangle$ and $|\downarrow\rangle$. The motional states act as the control qubit and the internal states as the target qubit for the gate. The control qubit is composed of the ground and second excited motional states ($n = 0, 2$) along the trap axis. The CNOT gate is operated by driving the carrier transition, which couples spin states with the same n. The laser-atom interaction is tuned so that an ion in the $|0\rangle$ state returns to its initial spin state while an ion in the $|2\rangle$ state toggles its spin state when the gate is driven. In the figure, filled circles represent two possible input ion eigenstates and open circles show the corresponding output state after the CNOT gate is applied.

and operations. As the number of ion qubits in a trap increases, several difficulties are encountered. For example, the addition of each ion adds three vibrational modes. It soon becomes nearly impossible to spectrally isolate the desired vibrational mode unless the speed of operations is slowed to an undesirable level [10, 26]. Furthermore, since error correction will most likely be incorporated into any large processor, it will be desirable to measure and reset ancillary qubits without disturbing the coherence of logical qubits. Since ion qubits are typically measured by means of state-dependent laser scattering, the scattered light from ancillary qubits held in a common trap may disturb the coherence of the logical qubits.

For these and other reasons, it appears that a scalable ion-trap quantum computer system must incorporate arrays of interconnected traps, each holding a relatively small number of ions. The information carriers between traps might be photons [27, 28, 29], or ions that are moved between traps in the array. In the latter case, a "head" ion held in a movable trap could carry the information by moving from site-to-site as in the proposal of Ref. [30]. Similarly, as has been proposed at NIST, we could shuttle ions around in an array of interconnected traps [10, 31]. In this last scheme, the idea is to transfer ions between nodes in the array by applying time-dependent potentials to "control" electrode segments. To perform logic operations between selected ions, these ions are transferred into an "accumulator" trap. Before the gate operation is performed, it may be necessary to re-cool the ions without disturbing their internal states. This could be accomplished by sympathetically cooling the qubit ions with another ion species [10]. Subsequently,

these ions are moved to memory locations or other accumulators. This strategy always maintains a relatively small number of motional modes that must be considered and minimizes the problems of ion/laser-beam addressing using focused laser beams. Such arrays also enable highly parallel processing and readout of ancillary qubits in separate trapping regions so that the logical ions are shielded from the scattered laser light. Some initial steps towards this scheme have been reported in Ref. [32].

FUNDAMENTAL TESTS, QUANTUM MEASUREMENT APPLICATIONS

The ability to coherently manipulate entangled quantum states, at least on a small scale, has enabled some demonstrations and tests of quantum mechanical principles that would have otherwise remained as gedanken experiments. For trapped ions, nonclassical motional states have been engineered by use of the basic elements of quantum computation [6, 11] and their properties determined through tomographic methods [33]. Schrödinger-cat states have been generated [34] and the scaling of their decoherence based on the size of the cat state has been verified [35, 36]. A scheme for generation of arbitrary motional states has recently been demonstrated on a single ion [37]. Entanglement of two and four separate ions has been generated deterministically ("on demand") [21, 38] without the need for post-selection, as in experiments using parametric down-conversion of photons. This enabled the first experiment showing a violation of Bell's inequalities (on massive particles) while defeating the "detection loophole" [39]. Treated as a small quantum processor, the trapped ion system can simulate the dynamics of other systems such as nonlinear optical beam splitters [40]. An exciting possibility is that these studies might eventually uncover some as-yet-unseen fundamental source of decoherence (see, for example, Ref. [41]).

One goal of the NIST experiments has been to use entanglement ("spin-squeezing") to increase the signal-to-noise ratio in spectroscopy and atomic clocks [8, 42]. An experiment on two ions has recently shown such squeezing [43] and, although not yet of practical use, the squeezing that was obtained led to a signal-to-noise ratio higher than could possibly be attained without entanglement on the same number of ions. Simple quantum processing might also be used to aid in quantum measurement readout with potential applications to mass spectroscopy [44] and frequency standards [45].

ACKNOWLEDGEMENTS

REFERENCES

H. Dehmelt, Science **247**, 539 (1990).
J. I. Cirac and P. Zoller, Phys. Rev. Lett. **74**, 4091 (1995).
D. P. DiVincenzo, Phys. Rev. A **51**, 1015 (1995).
A. Barenco *et al.*, Phys. Rev. A **52**, 3457 (1995).
D. P. DiVincenzo, in *Scalable Quantum Computers*, edited by S. L. Braunstein and H. K. Lo (Wiley-VCH, Berlin, 2001), pp. 1–13.
C. Roos *et al.*, Phys. Rev. Lett. **83**, 4713 (1999).
7. J. M. Raimond, M. Brune, and S. Haroche, Rev. Mod. Phys. **73**, 565 (2001).
8. D. J. Wineland *et al.*, Phys. Rev. A **46**, R6797 (1992).
9. F. Mintert and C. Wunderlich, Phys. Rev. Lett. **87**, 257904 (2001).
10. D. J. Wineland *et al.*, J. Res. Nat. Inst. Stand. Tech. **103**, 259 (1998).
11. D. M. Meekhof *et al.*, Phys. Rev. Lett. **76**, 1796 (1996).
12. F. Diedrich *et al.*, Phys. Rev. Lett. **62**, 403 (1989).
13. C. Monroe *et al.*, Phys. Rev. Lett. **75**, (1995).
14. C. F. Roos *et al.*, Phys. Rev. Lett. **85**, 5547 (2000).
15. H. Dehmelt, Ann. Phys. Fr. **10**, 777 (1985).
16. R. Blatt and P. Zoller, Eur. J. Phys. **9**, 250 (1988).
17. C. Monroe *et al.*, Phys. Rev. Lett. **75**, 4714 (1995).
18. A. Sørensen and K. Mølmer, Phys. Rev. Lett. **82**, 1971 (1999).
19. A. Sørensen and K. Mølmer, Phys. Rev. A **62**, 02231 (2000).
20. E. Solano, R. L. de Matos Filho, and N. Zagury, Phys. Rev. A **59**, 2539 (1999).
21. C. A. Sackett *et al.*, Nature **404**, 256 (2000).
22. D. Kielpinski *et al.*, Science **291**, 1013 (2001).
23. C. Monroe *et al.*, Phys. Rev. A **55**, R2489 (1997).
24. B. DeMarco *et al.*, quant-ph/0208180, Phys. Rev. Lett., to be published .
25. C. Sackett, Quant. Inform. Comp. **1**, 57 (2001).
26. A. M. Steane and D. M. Lucas, in *Scalable Quantum Computers*, edited by S. L. Braunstein, H. K. Lo, and P. Kok (Wiley-VCH, Berlin, 2000), pp. 69–88.

27. J. I. Cirac, P. Zoller, H. J. Kimble, and H. Mabuchi, Phys. Rev. Lett. **78**, 3221 (1997).
28. T. Pellizzari, Phys. Rev. Lett. **79**, 5242 (1997).
29. R. G. DeVoe, Phys. Rev. A **58**, 910 (1998).
30. J. I. Cirac and P. Zoller, Nature **404**, 579 (2000).
31. D. Kielpinski, C. Monroe, and D. J. Wineland, Nature **417**, 709 (2002).
32. M. A. Rowe *et al.*, Quant. Inform. Comp. **2**, 257 (2002).
33. D. Leibfried *et al.*, Phys. Rev. Lett. **77**, 4281 (1996).
34. C. Monroe, D. M. Meekhof, B. E. King, and D. J. Wineland, Science **272**, 1131 (1996).
35. C. J. Myatt *et al.*, Nature **403**, 269 (2000).
36. Q. A. Turchette *et al.*, Phys. Rev. A **62**, 053807 (2000).
37. A. Ben-Kish *et al.*, quant-ph/0208181, Phys. Rev. Lett., to be published .
38. Q. A. Turchette *et al.*, Phys. Rev. Lett. **81**, 1525 (1998).
39. M. A. Rowe *et al.*, Nature **409**, 791 (2001).
40. D. Leibfried *et al.*, Phys. Rev. Lett. **89**, 247901 (2002).
41. A. J. Leggett, Physics World **12**, 73 (1999).
42. J. J. Bollinger, W. M. Itano, D. J. Wineland, and D. J. Heinzen, Phys. Rev. A **54**, R4649 (1996).
43. V. Meyer *et al.*, Phys. Rev. Lett. **86**, 5870 (2001).
44. D. J. Heinzen and D. J. Wineland, Phys. Rev. A **42**, 2977 (1990).
45. D. J. Wineland *et al.*, in *Proc. 6th Symposium Frequency Standards and Metrology*, edited by P. Gill (World Scientific, Singapore, 2002), pp. 361–368.